

RSC Advances



This is an *Accepted Manuscript*, which has been through the Royal Society of Chemistry peer review process and has been accepted for publication.

Accepted Manuscripts are published online shortly after acceptance, before technical editing, formatting and proof reading. Using this free service, authors can make their results available to the community, in citable form, before we publish the edited article. This *Accepted Manuscript* will be replaced by the edited, formatted and paginated article as soon as this is available.

You can find more information about *Accepted Manuscripts* in the [Information for Authors](#).

Please note that technical editing may introduce minor changes to the text and/or graphics, which may alter content. The journal's standard [Terms & Conditions](#) and the [Ethical guidelines](#) still apply. In no event shall the Royal Society of Chemistry be held responsible for any errors or omissions in this *Accepted Manuscript* or any consequences arising from the use of any information it contains.

ARTICLE

Gold Nanoparticles Immobilized on Crystalline Titanate Fibres and Shuttling Effect of Charges in Solar Photocatalysis

Cite this: DOI: 10.1039/x0xx00000x

Received 00th September 2014,
Accepted 00th September 2014

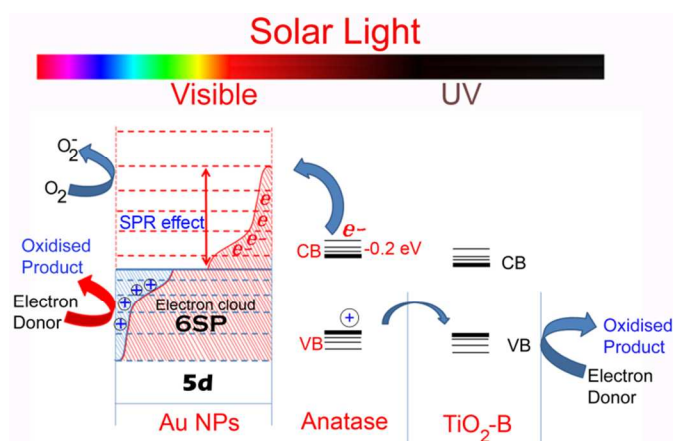
DOI: 10.1039/x0xx00000x

www.rsc.org/

Blain Paul ^a, Kwang-Ho Choo ^{a,b,*}, Gajanan S. Ghodake ^b, Daesung Lee ^b

This study focuses on understanding the intriguing nature of charge transfer processes between immobilized gold nanoparticles (AuNPs) and bi-crystalline titanate nanofibre substrates in solar light photocatalysis. Colloidal AuNPs with an average diameter of 20 nm were stably immobilized on titanate bi-crystals via casein-derived peptide linkers. The peptide linking method was adopted in order to attach the same amount of AuNPs onto two different bi-crystalline titanate fibres, i.e., H-titanate fibres with anatase patches ($\text{Ti}^{\text{H-A}}$) and $\text{TiO}_2\text{-B}$ fibres with anatase patches ($\text{Ti}^{\text{B-A}}$). The peptide cap surrounding the AuNPs was removed by combustion at 200°C, leaving the AuNPs firmly bound to the titanate fibres. A pronounced charge transfer effect was observed in the photocatalysis investigation of the two types of bi-crystalline fibres. Facile shuttling of photoexcited charges between the anatase sheathed $\text{TiO}_2\text{-B}$ fibres and AuNPs contributed significantly to the solar photocatalytic performance. In contrast, anatase sheathed H-titanate fibres were ineffective for enhancing the photoactivity after immobilization of gold particles. H-titanate and $\text{TiO}_2\text{-B}$ phases are known to be photocatalytically inactive under visible irradiation; however, alignment of the conduction band of $\text{TiO}_2\text{-B}$ with anatase in the decorated fibres facilitated shuttling of charges by precluding fast recombination of electrons and holes. When the $\text{TiO}_2\text{-B}$ phase was present in the bi-crystals, solar driven photocatalysis was enhanced, as evidenced by phenol degradation and photocurrent measurements.

Graphical Abstract



INTRODUCTION

The solar energy delivered to the Earth's surface in one hour is sufficient to fulfil our energy needs for one year.¹ In the daylight spectrum, UV light ($\lambda < 400$ nm) constitutes <4% of sunlight, while visible light accounts for >43%.² Trapping sunlight in chemical systems is proposedly one of the best solutions to resolve the world's energy crisis; thus, the synthesis of new materials and devising novel systems to trap the wide spectrum of solar light is very attractive.³ Numerous studies have focused on the design of semiconductor photocatalysts with specific shapes and functions for light concentration and utilization. However, when these materials are refined to nanoscale dimensions, unwanted or abnormal behaviours are evoked due to restricted electron motion under size and shape restrictions.^{2, 4-8} Many of the efforts to improve visible light activity based on new molecular designs have ended up with opposite results, whereas a key milestone was achieved by

minor modification of the photocatalyst without significantly modifying the base material.^{4,9}

TiO₂ based semiconductors are the most stable and highly reactive photocatalysts, but are only active under UV irradiation. Several successful approaches to absorb visible light with these catalysts have been reported and categorized as follows:^{4, 10-14} substitution or interstitial doping with C, F, N, P, and transition metals; photosensitization by dyes and metals; noble metal loading (e.g., Pt, Au). Noble metals that are photo-chemically deposited onto various titania substrates (e.g., nanofibres, nanotubes) accelerate the transfer of photo-excited electrons from titania to the surface. These noble metals can act as reaction centres (e.g., hydrogen evolving centres in water splitting cells) and also absorb visible light by plasmon resonance.¹⁵⁻¹⁸ Photo-excited electrons in the conduction band (CB) of titania are localized in the presence of gold nanoparticles (AuNPs); thus, the recombination of electrons to the valence band (VB) is delayed, as has been verified by time resolved microwave conductivity measurements.¹⁹ The localized electrons in AuNPs are effectively absorbed by molecular oxygen in the form of highly reactive superoxides resulting in significantly enhanced photocatalytic activity.²⁰ Several previous findings have reported plasmonic activity of AuNPs when present in solution as well as in a solid matrix.²¹⁻²⁵ It was recently reported that AuNPs loaded on TiO₂ were capable of electron injection into TiO₂ under visible irradiation due to surface plasmon resonance.¹⁷ When noble metal nanoparticles (e.g., Au or Ag) are exposed to light, a series of photochemical processes occur within the particles. The absorbed energy is rapidly converted to heat.²⁶⁻²⁸ The rate of heat release is a local effect, but charge transfer is related to the substrate on which the co-catalysts are fixed.^{29, 30} Light-induced heat generation by AuNPs has some plasmonic applications, including surface modification and phase transitions.^{31, 32} The interfacial charge transfer induced by the noble metal particles influences the chemical reactions depending on the environmental conditions.^{33, 34} The catalytic behaviour of noble metal particles is also affected by their size and shape.^{35, 36}

The primary aim of the present study is to investigate the effect of the type of phases used as support materials on the photocatalytic activity of AuNPs immobilized on mixed-phase TiO₂ structures. Herein, the preparation of stable colloidal AuNPs is performed using casein hydrolytic peptides with carboxylic and amino groups. The decoration of colloidal AuNPs onto two different bi-crystalline titanate frameworks is conducted via a peptide linker, and the morphological, spectral, and photocatalytic characteristics of the AuNP decorated titanate bi-crystals are evaluated and compared in the absence of interfacial peptide capping. The triple and quadruple layered catalyst designs are anticipated to find applicability in techniques suitable for harvesting solar light in photochemical systems based on the insight provided in this report.

MATERIALS AND METHODS

Chemicals

The starting reagents for the preparation of gold particles and titania fibres were all purchased from Sigma–Aldrich and were used as received.

Preparation of gold nanoparticles and bi-crystalline fibres

In a typical preparation of gold nanoparticles, 3.0 mL of 0.5% (wt) casein hydrolytic peptides (Sigma-Aldrich, USA) and 0.1 mL of 1 M NaOH were added to 15.4 mL water and incubated at 60 °C for 1.0 h to reach the operational temperature; a 1.5 mL aliquot of a 20 mM solution of gold salt (HAuCl₄) was subsequently added. The reaction mixture (20 mL) was maintained at 60 °C for 48 h. A colour change of the solution to light red indicated the formation of gold nanoparticles. The method used to produce the casein hydrolytic peptide-assisted gold nanoparticles is simple and highly reproducible.

Synthesis of the bi-crystalline titanate is based on a previously reported method.^{37, 38} First, 6 g of P25 in 80 mL of 10 M NaOH solution was vigorously stirred for 1 h and then transferred into a Teflon-lined autoclave for 48 h of hydrothermal treatment at 180 °C. After cooling to room temperature, the precipitate was washed with deionized water and vacuum dried. Finally, the obtained H-titanate (Ti^H) was sheathed with anatase by an acid treatment; the acid treated substrate is termed 'Ti^{H-A}'. The acid treatment was performed as follows: H-titanate (0.8 g) was placed in 0.05 M HNO₃ (80 mL) at 110 °C for 40 h. Through further calcination at 450 °C for 4 h, the core H-titanate phase (Ti^H) was converted to TiO₂-B. This modified structure is designated as 'Ti^{B-A}'.

The obtained bi-crystalline titanate fibres (0.3 g) were further treated with 2% HF for 30 s (to create H-terminated surfaces) followed by washing with deionized water for 60 s. The product with H-terminated surfaces was thoroughly shaken with 12 mL of a colloidal solution of AuNPs for 6 h, filtered for collection, and finally dried in an oven at 80 °C for 24 h. The resulting product was calcined at 200 °C for 2 h in air to remove the surface capping (i.e., peptide) of the AuNPs. The anatase decorated H-titanate catalyst after immobilization of AuNPs is designated as Ti^{H-A}Au^{NP}. The uncapped anatase sheathed TiO₂-B fibres prepared in a similar manner are designated as Ti^{B-A}Au^{NP}.

Characterization of bi-crystalline titanate and gold nanoparticles

TEM images were acquired using a Hitachi H-7600 microscope at an accelerating voltage of 120 kV. XRD patterns were recorded using CuK α radiation ($n = 1.5418 \text{ \AA}$) on a Rigaku D/Max-2500 X-ray diffractometer operated at 40 kV and 100 mA, at a scanning speed of 6 degree/min, in the scan range of 10-80 degrees. Fourier transform infrared spectroscopy (FTIR) data were recorded on a PerkinElmer FTIR instrument (Spectrum GX & AutoImage). The UV-visible diffuse reflectance spectra (UV-DRS) of powder samples were measured using a UV-2450 Shimadzu spectrophotometer. The electron paramagnetic resonance (EPR) spectra (first derivative of the absorption curve) were recorded at 130 K using a JEOL JES-TE 300 spectrometer which was operated at 100 kHz field modulation and 1 mW microwave power. The sweep time was 4 min. The g values were determined using a di(phenyl)-(2,4,6-trinitrophenyl)iminoazanium standard. The absorbance spectra of the colloidal AuNPs were measured using a UV-visible spectrophotometer (Model 8453, Agilent).

Evaluation of photocatalytic activity

Phenol was used to evaluate the photocatalytic activities of the fabricated catalysts. The catalyst (0.5 g/L) was added to a 10 mg/L phenol solution. The reaction was performed in a completely mixed reactor. Aqueous samples were irradiated using a xenon arc lamp operated at 150 W (Model 13014, Ushio). The light exit of the xenon arc lamp housing was set 35 cm away from the surface of the solution in a Pyrex-glass reactor in order to illuminate with a light intensity equivalent to 'one sun' (0.1 W/cm^2). The phenol concentration was determined using a high performance liquid chromatograph (SPD-20A, Shimadzu Corp., Japan) equipped with a C18 column (Discovery®).

Photocurrent experiments were carried out on an inert working electrode (Pt) immersed in an aqueous suspension of photocatalyst (0.5 g/L, 0.95 N NaOH) using methyl viologen (MV^{2+} , 0.5 mM) as an electron shuttle, as previously discussed in the literature.³⁹ A saturated calomel electrode and a graphite rod were used as reference and counter electrodes, respectively. The suspension was purged for 30 min using nitrogen gas before being exposed to the 150 W Xe light source.

RESULTS AND DISCUSSION

Synthesis and spectroscopic characterization of gold nanoparticles and titanate bi-crystals

Casein hydrolytic peptides were used as reducing and capping agents during the synthesis of AuNPs under alkaline conditions. The carboxylic groups present in casein peptides may facilitate the complexation of metal ions. The amino acid residues present in the peptide solution donate electrons to the gold ions and thereby create Au^0 nanoparticles. Capping of AuNPs by the peptides can be accomplished by hydrogen bonds involving the amino and carboxylic groups, which form N–Au and O–Au bonds, respectively. The amino groups of the peptides may stabilize the AuNPs via hydrogen bonding while establishing cross-linking.

The colloidal AuNPs produced by the eco-friendly procedure described above are shown in Fig. 1. The AuNPs were stable with an average size distribution of around 20 nm in diameter and exhibited strong plasmonic resonance at a wavelength of 530 nm (Figure 1b). Because the particle size is much smaller than the wavelength of light, the AuNPs may exhibit unique light harvesting properties. Illumination of the AuNPs induces electron polarization on one spot of the gold surface; the polarization then moves to another spot, resulting in standing resonance oscillation. The oscillation of electron clouds imparts an intense pink colour to the colloidal solution of the metallic AuNPs.⁴⁰ In this study, AuNPs were attached to bi-crystalline titanate substrates for efficient harvesting of solar light. In the colloidal gold solution, the capping material (e.g., casein hydrolytic peptide) surrounding the AuNPs helps prevent aggregation of the AuNPs. In addition, the peptide cap acts as a linker for immobilization when the AuNPs are loaded onto the OH

terminated titanate substrate (which will be further discussed in a later section). OH-termination of the anatase-sheathed H-titanate (designated as $\text{Ti}^{\text{H-A}}$) and anatase-sheathed TiO_2 -B (designated as $\text{Ti}^{\text{B-A}}$) nanofibres was carried out as follows: titanate nanofibres were immersed in 2% HF for 30 s to replace some of the Ti–O–Ti bonds by Ti–F bonds.^{41, 42}

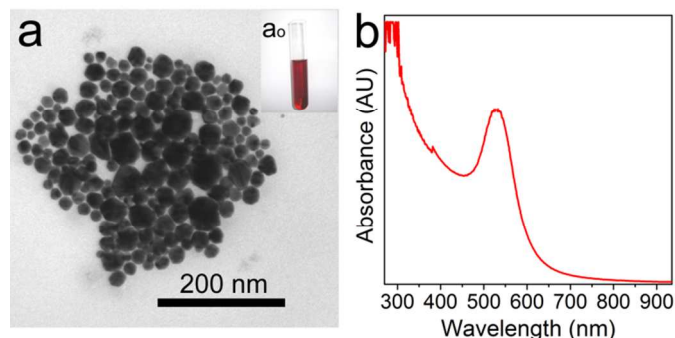


Fig. 1. (a) TEM images of the colloidal AuNPs synthesized. The inset (a') shows the dark pink colour of AuNPs in colloidal form. (b) UV-visible absorption spectrum of the AuNPs.

Hydrolysis of the F-terminated surface was achieved by exposure of the sample to pure water for 60 s, and the resulting Ti–OH bonds were detected with the aid of FTIR (Fig. 2). The FTIR spectrum of the $\text{Ti}^{\text{H-A}}$ sample washed with HF shows the presence of a very strong and broad band around 3500 cm^{-1} that is associated with the stretching vibration of Ti–O–H, and a small sharp band around 1600 cm^{-1} that is related to deformation of physically absorbed water.^{43, 44} Furthermore, a strong but broad band at $\sim 800 \text{ cm}^{-1}$, which is associated with Ti–O–H deformation, was observed.⁴⁵

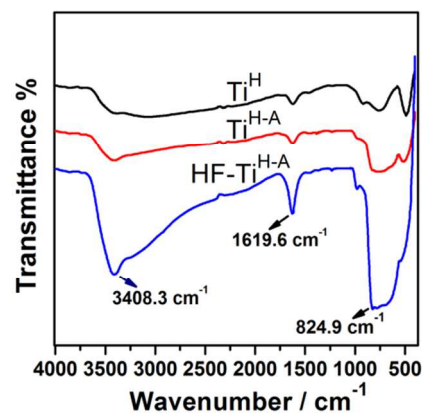


Fig. 2. FTIR spectra of H-titanate (Ti^{H}) and modified frameworks before (designated as $\text{Ti}^{\text{H-A}}$) and after (designated as $\text{HF-Ti}^{\text{H-A}}$) HF treatment followed by hydrolysis.

Examination of bi-crystalline titanate structures

The OH terminal of the bi-crystalline fibres with two different structures ($\text{Ti}^{\text{H-A}}$ and $\text{Ti}^{\text{B-A}}$) was further treated with colloidal gold solution. The titanate nanofibres loaded with gold particles were thus formed and designated as $\text{Ti}^{\text{H-A}}\text{Au}^{\text{NP}}$ and $\text{Ti}^{\text{B-A}}\text{Au}^{\text{NP}}$. The peptide layer between the titanate nanofibres and AuNPs was removed by

heating at 200°C. Finally, the co-existence of two titania solid phases in the bi-crystalline framework containing gold co-catalysts was examined by XRD (Fig. 3). Peaks of pure H-titanate (Ti^{H}) were observed at 2θ values of 8.1°, 11.2°, 24.7°, 28.02°, 34.5°, and 48.22°. The major diffraction peaks were readily identified for the samples of $\text{Ti}^{\text{H-A}}\text{Au}^{\text{NP}}$ and $\text{Ti}^{\text{B-A}}\text{Au}^{\text{NP}}$, suggesting the formation of anatase patches on the core fibres. It is clear that $\text{Ti}^{\text{H-A}}\text{Au}^{\text{NP}}$ possesses the same bi-crystalline structure (H-titanate core + anatase sheath) as that of $\text{Ti}^{\text{H-A}}$. The peak corresponding to the anatase phase was slightly more intense in the case of $\text{Ti}^{\text{B-A}}\text{Au}^{\text{NP}}$, and peaks associated with the $\text{TiO}_2\text{-B}$ phase appeared at 14.28° and 28.96°. No peaks related to H-titanate (Ti^{H}) were detected for $\text{Ti}^{\text{B-A}}\text{Au}^{\text{NP}}$, i.e., the peaks at 7.9° and 11.22° disappeared during the calcination process. The diffraction pattern of $\text{Ti}^{\text{B-A}}\text{Au}^{\text{NP}}$ clearly demonstrates the bi-crystalline characteristics in which anatase is present over the $\text{TiO}_2\text{(B)}$ phases.

The UV-visible absorption spectra of the bi-crystalline titanate fibres with and without AuNP decoration are shown in Fig. 3b. All gold decorated samples possess absorption edges extending into the visible region. The UV-visible spectra of the gold embedded titanate fibres show two distinct absorption bands: one is in the visible region at ~550 nm and the other is in the UV region with a strong absorption at ~370 nm. The absorption in the visible spectral range is attributed to the surface plasmonic effect of the AuNPs. Careful examination of the position of the surface plasmon band of the AuNP decorated samples revealed a slight red shift in the absorption from that of the colloidal solution at 530 nm. Because the plasmonic resonance is a surface phenomenon, the red shift of absorption of the AuNPs on the titanate bi-crystals could be ascribed to their close contact with the anatase substrate (i.e., facile charge transfer through the AuNPs). Gold particles could effectively take part in the solar light photocatalysis by transferring photoexcited charges via various mechanisms; the contribution of the AuNPs to the enhanced photocatalytic activity is discussed in a later section.

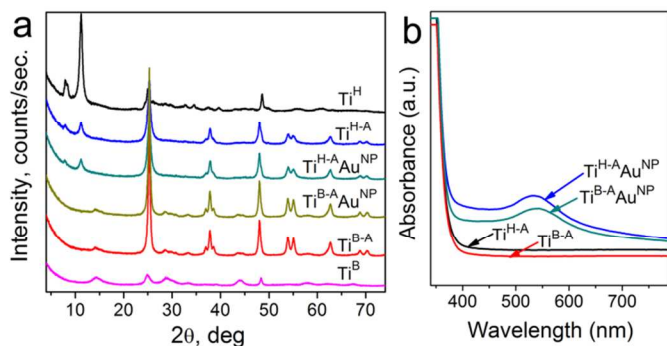


Fig. 3. (a) XRD patterns of various titanate nanofibres with different crystal structures. $\text{Ti}^{\text{H-A}}$ and $\text{Ti}^{\text{H-A}}\text{Au}^{\text{NP}}$ have the H-titanate phase (Ti^{H}) in their core with patches of the anatase phase, whereas $\text{Ti}^{\text{B-A}}\text{Au}^{\text{NP}}$ contains the $\text{TiO}_2\text{-B}$ (Ti^{B}) phase in its core with anatase patches. (b) UV-visible absorption spectra of titanate fibres with and without gold nanoparticle decoration.

The morphology and microstructural details related to the surface of bi-crystalline Ti^{BA} and $\text{Ti}^{\text{B-A}}\text{Au}^{\text{NP}}$ are shown in Fig. 4. The TEM

image (Fig. 4a) clearly shows the surface topography of the nanofibres (Ti^{BA}) before loading the AuNPs. It can be seen that crystalline fibres subjected to acid treatment have an uneven surface; the induced surface roughness in most plausibly due to the formation of anatase patches through acid hydrolysis of the core fibres. The AuNPs embedded onto the titanate fibres can be clearly visualized in the TEM images.

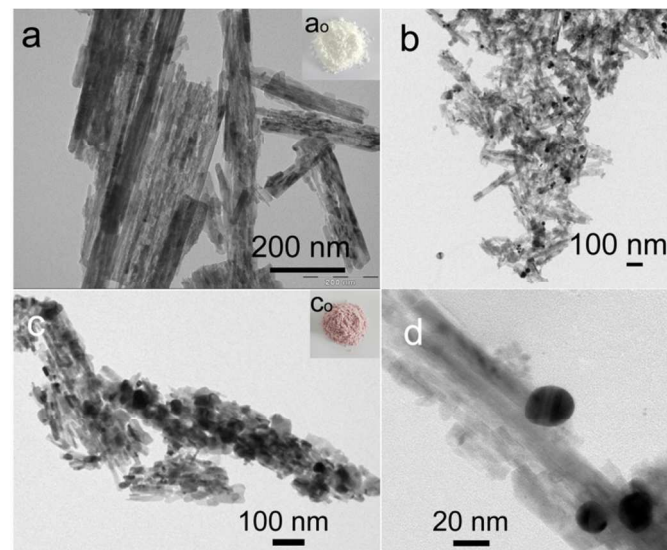


Fig. 4. High magnification TEM image (a) and photograph (a₀) of pure powder sample of Ti^{BA} before loading with AuNPs; (b), (c) and (d) show TEM images of $\text{Ti}^{\text{B-A}}\text{Au}^{\text{NP}}$ at different magnifications. (c₀) Photograph of a $\text{Ti}^{\text{B-A}}\text{Au}^{\text{NP}}$ sample after loading AuNPs on $\text{Ti}^{\text{A-B}}$.

Electron paramagnetic resonance characteristics

EPR spectroscopy can be used to identify various trap sites for photo-generated electrons and holes. Fig. 5 shows the difference in the EPR signals of two different samples before and after exposure to artificial sunlight. The powder samples were exposed to light under atmospheric conditions for 600 s to generate paramagnetic species; spectra were then acquired at 140 K. Upon photoexcitation, the electrons are primarily trapped at the coordinated cations to form Ti^{3+} , whereas the holes are trapped on the lattice oxygen atoms to form $\text{Ti}^{4+}\text{-O}^{\cdot}$. Signals are observed at $g = 2.004$ and $g = 1.959$ in the EPR spectra; these signals are respectively due to the photo-generated holes and electrons that accumulated at the trapping sites of anatase.⁴⁹⁻⁵¹ The electron and hole signals of $\text{Ti}^{\text{H-A}}\text{Au}^{\text{NP}}$ became slightly more intense after photo-irradiation. The valence and conduction bands of the H-titanate and anatase phases associated with $\text{Ti}^{\text{H-A}}\text{Au}^{\text{NP}}$ were impossible to align for any kind of interfacial charge transport.^{52, 53} Consequently, the electrons and holes were trapped on the lattice. Gold nanoparticles can undergo interfacial charge transfer, but no such effect was observed with $\text{Ti}^{\text{H-A}}\text{Au}^{\text{NP}}$ due to fast recombination. Upon photo-irradiation, the intensity of the signals derived from the trapped holes and electrons increase markedly for $\text{Ti}^{\text{H-A}}\text{Au}^{\text{NP}}$. The intensity of the signal for $\text{Ti}^{\text{H-A}}\text{Au}^{\text{NP}}$ (a_2) in Fig. 5 increased by a factor of ~2 when compared to that

before photo-irradiation (a_1), indicating effective trapping of holes in $\text{Ti}^{\text{H-A}}\text{Au}^{\text{NP}}$. Unlike $\text{Ti}^{\text{H-A}}\text{Au}^{\text{NP}}$, the weaker signal for $\text{Ti}^{\text{B-A}}\text{Au}^{\text{NP}}$ after photo-irradiation (b_2) is possibly due to its facile migration from anatase to the inner core of the $\text{TiO}_2\text{-B}$ phases where the bands are aligned with each other.⁵⁴ This behaviour may provide enough time for transfer of electrons to the AuNPs.

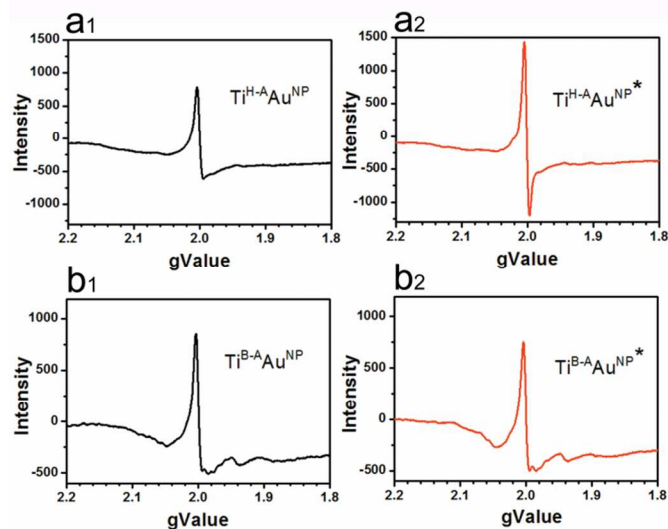


Fig. 5. A comparison of g values for the paramagnetic spin resonance spectra of air saturated samples observed before (left) and after (*right) artificial sunlight irradiation; a_1 and a_2 : $\text{Ti}^{\text{H-A}}\text{Au}^{\text{NP}}$; b_1 and b_2 : $\text{Ti}^{\text{B-A}}\text{Au}^{\text{NP}}$.

Enhanced photocatalytic activity and mechanisms

The oxidative decomposition of phenol was evaluated in order to compare the solar photocatalytic efficiency of photoinduced charge carriers generated in the different bi-crystalline titanate fibres decorated with plasmonic AuNPs (Fig. 6a). Figure 6b shows the time profiles of the collected current for different samples in aqueous suspension under solar irradiation, which indicates the same trend as observed for the performance of the catalysts in the degradation of phenol. The photocurrent of $\text{Ti}^{\text{B-A}}\text{Au}^{\text{NP}}$ reached a saturation value around 0.12 mA, which was the highest value obtained for the samples tested under the same conditions. The plateau of the photocurrent curve demonstrates the ability of the catalyst to generate photoexcited species and can be used to predict the photocatalytic efficiency of the material. Photocurrent measurement is a versatile tool for understanding the mechanism of photo-oxidation reactions; indeed, the effectiveness of the reaction is strictly linked to the formation of photoexcited charge carriers and recombination. The increase in the saturation value of the photocurrent signals for $\text{Ti}^{\text{B-A}}\text{Au}^{\text{NP}}$ demonstrates that the gold particles contribute to the electron-hole excitations. It also highlights the fact that decoration of a proper substrate with AuNPs could deliver significantly enhanced photocurrent responses.

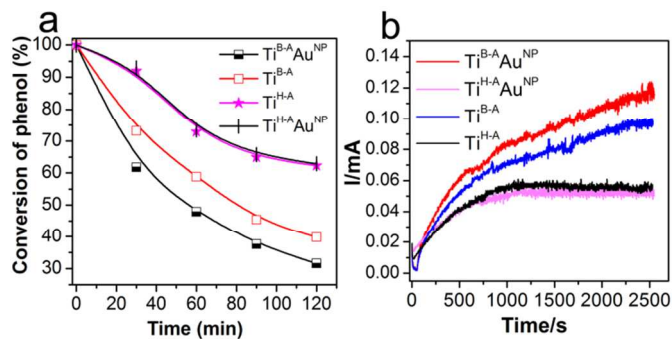


Fig. 6. (a) Efficiency of photocatalytic degradation of phenol with various catalysts. (b) Photocurrents measured at room temperature.

The schematic illustration presented in Fig. 7 is used to explain the possible pathways of charge carrier transport that contribute to the photocatalytic efficiency of $\text{Ti}^{\text{B-A}}\text{Au}^{\text{NP}}$. As seen in Figure 6a, the most substantial decomposition of phenol occurred with $\text{Ti}^{\text{B-A}}\text{Au}^{\text{NP}}$, which has a structure comprising $\text{TiO}_2\text{-B}$ fibres with patches of anatase decorated with AuNPs. The highest photocatalytic efficiency demonstrated by $\text{Ti}^{\text{B-A}}\text{Au}^{\text{NP}}$ is attributable to the facile transport of charge carriers into the inner core of the $\text{TiO}_2\text{-B}$ phase. $\text{Ti}^{\text{H-A}}\text{Au}^{\text{NP}}$ is composed of a H-titanate inner core, whereas $\text{Ti}^{\text{B-A}}\text{Au}^{\text{NP}}$ comprises a $\text{TiO}_2\text{-B}$ core which would facilitate the transport of charge carriers from anatase to $\text{TiO}_2\text{-B}$. The bandgap energy of $\text{TiO}_2\text{-B}$ (~ 3.0 eV) is narrower than that of anatase (~ 3.2 eV),⁵⁴ which allows ready transport of charge carriers from anatase patches to the core, resulting in an improved separation of excitons.^{55, 56} The photon energy associated with visible light is much lower than that of UV light. Surface plasmonic resonance (SPR) effects occurred on conduction of electrons in the 6sp energy levels under visible light irradiation of the AuNPs. The electrons in the 6sp energy levels are excited and redistributed to higher levels in the 6sp bands above the Fermi level after absorbing energy from visible light. The excited electrons are available to interact with molecular oxygen, and positively charged holes are left behind in the lower 6sp energy levels after migration of the electrons to higher levels. The excited electrons remain in higher energy levels for up to 1–0.5 picoseconds.⁵⁷ The positively charged holes are available to capture electrons from organic species. However, the oxidising power to attack organic species may vary depending on the reduction potential associated with the holes. The generation of positively charged holes and the reduction potential of the holes are directly related to the wavelength of visible light from which the holes are generated due to electron migration to higher levels. Furthermore, the ability of AuNPs to absorb a particular wavelength of light is associated with the shape and size of the particles.⁵⁸ Thus, the generated holes possess particular reduction potentials depending on the wavelength of light. It is clear that not all organic species can be oxidised with generation of holes from plasmonic effects. Some organic molecules such as phenol cannot be oxidised with the generation of holes using visible light, and the holes generated by UV light is only suitable for the destruction of such molecules.⁵⁹

As seen in Figure 7, when the plasmonic AuNPs are in direct contact with the anatase phase, charge transfer from the AuNPs to the metal and vice versa is operative.⁶⁰⁻⁶² The transfer of excited electrons between the AuNPs and semiconductors occurs when there is such an alignment. The Fermi levels of the AuNPs (+0.45 V versus NHE) and TiO₂ (Fermi value of bare TiO₂ = -0.23 V) are aligned with each other when both are in contact.⁶² The Fermi levels eventually shift to become close to the conduction band of anatase. The excited plasmonic electrons on the AuNPs remain in the higher energy levels only for a fraction of a second given that the plasmonic effect is the oscillation of electrons. Thus, recombination of the electrons on anatase is delayed, the excited electrons can easily be transferred to the AuNPs (route 3), and those electrons are potentially available to interact with molecular oxygen (route 2). The delay of recombination is facilitated in Ti^{B-A}Au^{NP} due to the transfer of holes to TiO₂-B (route 4). A different scenario is applicable to phenol degradation and photocurrent experiments with Ti^{H-A}Au^{NP}. Unlike Ti^{B-A}Au^{NP}, the transport of photoexcited charges from anatase to the H-titanate core is hindered in Ti^{H-A}Au^{NP} due to the wide bandgap (3.4–3.8 eV) of H-titanate.^{52, 53} In the absence of charge transport from anatase to the H-titanate phase, photoexcited electrons accumulate in the conduction band, which causes back reactions and fast recombination. Fast recombination precludes electron migration (route 3) from the conduction bands of anatase to higher energy levels of the gold particles. Hence, the electrons are not available to interact with molecular oxygen.

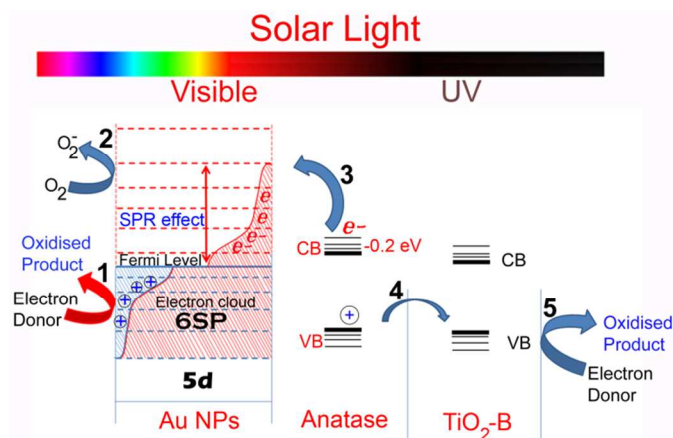


Fig. 7. Schematic illustration of the photocatalysis process showing the proposed structural arrangements and possible charge carrier transport pathways associated with Ti^{B-A}Au^{NP}.

Conclusions

Two different photocatalytic designs with anatase patches on either TiO₂-B fibres or H-titanate fibres decorated with AuNPs were used to illustrate the mechanism for improving the efficiency of sunlight harvesting using AuNPs. AuNPs were synthesised via reduction of gold ions (Au³⁺) by casein hydrolytic peptides, which enabled the production of stable gold nanoparticle colloids. Decoration of the nanofibres composed of two different bi-crystalline titanate phases (anatase on H-titanate core and anatase on TiO₂-B) with colloidal AuNPs was successfully achieved. Linking between AuNPs and

titania was achieved by exploiting peptides as a capping agent for the AuNPs. The interfacial peptide layer functioned as a bridge between the AuNPs and bi-crystalline nanofibres, and was later removed by heating at 200 °C. Enhanced photoactivity was observed for the design comprising anatase patches on TiO₂-B fibres decorated with AuNPs. This high performance is attributed to the transport of photogenerated electrons and holes with minimal recombination due to facile charge exchange with TiO₂-B. The design comprising anatase patches on H-titanate fibres decorated with AuNPs showed a strong EPR signal after photo-irradiation; however, the photocatalytic performance of this design was slightly lower than that of bare fibres. During photo-excitation of anatase, electrons accumulate in the valence band, resulting in back-transfer and fast recombination of excited charges due to the lack of transport through the H-titanate core.

Acknowledgements

This research was supported by the National Research Foundation of Korea funded by the Korean Government (2010-0014848 and 2012H1B8A2026280). The authors express thanks to Prof. H. Park and Mr. K.S. Choi for their assistance with photocurrent measurements.

Notes and references

^aAdvanced Institute of Water Industry, Kyungpook National University, 80 Daehak-ro, Buk-gu, Daegu 702-701, Republic of Korea.

^bDepartment of Environmental Engineering, Kyungpook National University, 80 Daehak-ro, Buk-gu, Daegu 702-701, Republic of Korea.

*E-mail: chookh@knu.ac.kr, Phone: +82-53-950-7585, Fax: +82-53-950-6579.

[†]Electronic Supplementary Information (ESI) available: [Experimental details]. See DOI: 10.1039/c000000x/

- O. Morton, *Nature*, 2006, 443, 19-22.
- Z. Zou, J. Ye, K. Sayama and H. Arakawa, *Nature*, 2001, 414, 625-627.
- J. K. McCusker, *Science*, 2001, 293, 1599-1601.
- R. Asahi, T. Morikawa, T. Ohwaki, K. Aoki and Y. Taga, *Science*, 2001, 293, 269-271.
- M. Anpo and M. Takeuchi, *J. Catal.*, 2003, 216, 505-516.
- S. Sato, *Chem. Phys. Lett.*, 1986, 123, 126-128.
- T. Ohno, M. Akiyoshi, T. Umebayashi, K. Asai, T. Mitsui and M. Matsumura, *Appl. Catal. A-Gen.*, 2004, 265, 115-121.
- Z. W. Seh, S. Liu, M. Low, S.-Y. Zhang, Z. Liu, A. Mlayah and M.-Y. Han, *Adv. Mater.*, 2012, 24, 2310-2314.
- B. O'Regan and M. Gratzel, *Nature*, 1991, 353, 737-740.
- T. Ohno, T. Tsubota, M. Toyofuku and R. Inaba, *Catal. Lett.*, 2004, 98, 255-258.
- W.-K. Jo and J. Y. Lee, *Environ. Eng. Res.*, 2013, 18, 21-28.
- J.-Y. Lee and W.-K. Jo, *Environ. Eng. Res.*, 2012, 17, 179-184.
- M. Pelaez, N. T. Nolan, S. C. Pillai, M. K. Seery, P. Falaras, A. G. Kontos, P. S. M. Dunlop, J. W. J. Hamilton, J. A. Byrne, K. O'Shea, M. H. Entezari and D. D. Dionysiou, *Appl. Catal. B-Environ.*, 2012, 125, 331-349.

14. S. Banerjee, S. C. Pillai, P. Falaras, K. E. O'Shea, J. A. Byrne and D. D. Dionysiou, *J. Phys. Chem. Lett.*, 2014, 5, 2543-2554.
15. A. Nitzan and L. E. Brus, *J. Chem. Phys.*, 1981, 75, 2205-2214.
16. C. J. Chen and R. M. Osgood, *Phys. Rev. Lett.*, 1983, 50, 1705-1708.
17. Y. Tian and T. Tatsuma, *J. Am. Chem. Soc.*, 2005, 127, 7632-7637.
18. R. S. Sonawane and M. K. Dongare, *J. Mol. Catal. A-Chem.*, 2006, 243, 68-76.
19. J. T. Carneiro, T. J. Savenije and G. Mul, *Phys. Chem. Chem. Phys.*, 2009, 11, 2708-2714.
20. C.-J. Liu, T.-Y. Yang, C.-H. Wang, C.-C. Chien, S.-T. Chen, C.-L. Wang, W.-H. Leng, Y. Hwu, H.-M. Lin, Y.-C. Lee, C.-L. Cheng, J. H. Je and G. Margaritondo, *Mater. Chem. Phys.*, 2009, 117, 74-79.
21. T. S. Ahmadi, S. L. Logunov and M. A. El-Sayed, *J. Phys. Chem.*, 1996, 100, 8053-8056.
22. T. Tokizaki, A. Nakamura, S. Kaneko, K. Uchida, S. Omi, H. Tanji and Y. Asahara, *Appl. Phys. Lett.*, 1994, 65, 941-943.
23. T. W. Roberti, B. A. Smith and J. Z. Zhang, *J. Chem. Phys.*, 1995, 102, 3860-3866.
24. R. H. M. Groeneveld, R. Sprik and A. Lagendijk, *Phys. Rev. Lett.*, 1990, 64, 784-787.
25. V. Rodríguez-González, R. Zanella, G. del Angel and R. Gómez, *J. Mol. Catal. A: Chem.*, 2008, 281, 93-98.
26. D. K. Roper, W. Ahn and M. Hoepfner, *J. Phys. Chem. C*, 2007, 111, 3636-3641.
27. M. A. El-Sayed, *Acc. Chem. Res.*, 2001, 34, 257-264.
28. P. V. Kamat, M. Flumiani and G. V. Hartland, *J. Phys. Chem. B*, 1998, 102, 3123-3128.
29. X. Chen, H.-Y. Zhu, J.-C. Zhao, Z.-F. Zheng and X.-P. Gao, *Angew. Chem. Int. Ed.*, 2008, 47, 5353-5356.
30. S. Link and M. A. El-Sayed, *Int. Rev. Phys. Chem.*, 2000, 19, 409-453.
31. L. Rontzsch, K. H. Heinig, J. A. Schuller and M. L. Brongersma, *Appl. Phys. Lett.*, 2007, 90.
32. A. O. Govorov, W. Zhang, T. Skeini, H. Richardson, J. Lee and N. A. Kotov, *Nanoscale Res. Lett.*, 2006, 1, 84-90.
33. M. D. Hughes, Y.-J. Xu, P. Jenkins, P. McMorn, P. Landon, D. I. Enache, A. F. Carley, G. A. Attard, G. J. Hutchings, F. King, E. H. Stitt, P. Johnston, K. Griffin and C. J. Kiely, *Nature*, 2005, 437, 1132-1135.
34. S. Link and M. A. El-Sayed, *Annu. Rev. Phys. Chem.*, 2003, 54, 331-366.
35. M. M. Schubert, S. Hackenberg, A. C. van Veen, M. Muhler, V. Plzak and R. J. Behm, *J. Catal.*, 2001, 197, 113-122.
36. T. S. Ahmadi, Z. L. Wang, T. C. Green, A. Henglein and M. A. El-Sayed, *Science*, 1996, 272, 1924-1925.
37. Z. F. Zheng, H. W. Liu, J. P. Ye, J. C. Zhao, E. R. Waclawik and H. Y. Zhu, *J. Mol. Catal. A-Chem.*, 2010, 316, 75-82.
38. Zhu, Gao, Y. Lan, Song, Xi and Zhao, *J. Am. Chem. Soc.*, 2004, 126, 8380-8381.
39. H. Park and W. Choi, *J. Phys. Chem. B*, 2003, 107, 3885-3890.
40. S. Eustis and M. A. El-Sayed, *Chem. Soc. Rev.*, 2006, 35, 209-217.
41. H. G. Yang and H. C. Zeng, *J. Phys. Chem. B*, 2003, 107, 12244-12255.
42. X. H. Yang, Z. Li, C. Sun, H. G. Yang and C. Li, *Chem. Mater.*, 2011, 23, 3486-3494.
43. G. Li, L. Li, J. Boerio-Goates and B. F. Woodfield, *J. Am. Chem. Soc.*, 2005, 127, 8659-8666.
44. M. Minella, M. G. Faga, V. Maurino, C. Minero, E. Pelizzetti, S. Coluccia and G. Martra, *Langmuir*, 2009, 26, 2521-2527.
45. P. K. Suroolia, M. A. Lazar, R. J. Tayade and R. V. Jasra, *Ind. Eng. Chem. Res.*, 2008, 47, 5847-5855.
46. Y. Mao, M. Kanungo, T. Hemraj-Benny and S. S. Wong, *J. Phys. Chem. B*, 2005, 110, 702-710.
47. R. Ma, K. Fukuda, T. Sasaki, M. Osada and Y. Bando, *J. Phys. Chem. B*, 2005, 109, 6210-6214.
48. A. R. Armstrong, G. Armstrong, J. Canales and P. G. Bruce, *Angew. Chem. Int. Ed.*, 2004, 43, 2286-2288.
49. T. Hirakawa, H. Kominami, B. Ohtani and Y. Nosaka, *J. Phys. Chem. B*, 2001, 105, 6993-6999.
50. J. H. Lunsford, *Adv. Catal.*, 1972, 22, 265-344.
51. I. R. Macdonald, S. Rhydderch, E. Holt, N. Grant, J. M. D. Storey and R. F. Howe, *Catal. Today*, 2012, 182, 39-45.
52. H. Yu, J. Yu and B. Cheng, *Chemosphere*, 2007, 66, 2050-2057.
53. D. V. Bavykin, J. M. Friedrich and F. C. Walsh, *Adv. Mater.*, 2006, 18, 2807-2824.
54. T. Hongo and A. Yamazaki, *Microporous Mesoporous Mat.*, 2011, 142, 316-321.
55. W. Li, C. Liu, Y. Zhou, Y. Bai, X. Feng, Z. Yang, L. Lu, X. Lu and K.-Y. Chan, *J. Phys. Chem. C*, 2008, 112, 20539-20545.
56. Z. Zheng, H. Liu, J. Ye, J. Zhao, E. R. Waclawik and H. Zhu, *J. Mol. Catal. A: Chem.*, 2010, 316, 75-82.
57. M. Haruta and M. Daté, *Appl. Catal. A-Gen.*, 2001, 222, 427-437.
58. E. Kowalska, O. O. P. Mahaney, R. Abe and B. Ohtani, *Phys. Chem. Chem. Phys.*, 2010, 12, 2344-2355.
59. H. Zhu, X. Chen, Z. Zheng, X. Ke, E. Jaatinen, J. Zhao, C. Guo, T. Xie and D. Wang, *Chem. Commun.*, 2009, DOI: 10.1039/B917052A, 7524-7526.
60. C. Gomes Silva, R. Juárez, T. Marino, R. Molinari and H. Garcia, *J. Am. Chem. Soc.*, 2010, 133, 595-602.
61. R. Jiang, B. Li, C. Fang and J. Wang, *Adv. Mater.*, 2014, 26, 5274-5309.
62. V. Subramanian, E. E. Wolf and P. V. Kamat, *J. Am. Chem. Soc.*, 2004, 126, 4943-4950.